Large-scale production of hierarchical iron rusts/$Ni(OH)_2$ nanosheet-on-microsphere arrays for efficient electrocatalysis

Xupo Liu,‡[a] Xuyun Guo,‡[b] Mingxing Gong,[a] Shaofeng Deng,[a] Jianing Liang,[a] Tonghui Zhao,[a] Yun Lu,[a] Tao Shen,[a] Ye Zhu,[b] Jian Zhang[a] and Deli Wang*[a]

[a]*Key Laboratory of Material Chemistry for Energy Conversion and Storage (Huazhong University of Science and Technology), Ministry of Education, Hubei Key Laboratory of Material Chemistry and Service Failure, School of Chemistry and Chemical Engineering, Huazhong University of Science and Technology, Wuhan, 430074, P.R. China. E-mail: wangdl81125@hust.edu.cn.*

[b]*Department of Applied Physics, The Hong Kong Polytechnic University, Hung Hom, Hong Kong, P. R. China.*

‡X. Liu and X. Guo contributed equally to the work.

Abstract: Iron corrosion is always harmful to our industrial manufacture and thus numerous effects have been conducted for corrosion protection. However, the detrimental corrosion may be applied to produce serviceable materials, resulting in "upcycling waste into wealth". Herein, a novel corrosion engineering is employed to fabricate hierarchical iron rusts/$Ni(OH)_2$ nanosheet-on-microsphere arrays as effective oxygen evolution reaction (OER) electrocatalysts. Through physically mixing the fabricated ultrathin iron rusts with $Ni(OH)_2$ microspheres, the as-prepared catalyst requires an overpotential of only 318 mV to achieve the current density of 20 mA cm^{-2}. Besides, negligible increasement of overpotential is observed after continuous chronopotentiometric determination for 30 h. The excellent OER property is attributed to the formed oxygen bridges of Fe-O-Ni on the solid-solid contact sites, which promote oxidation of Ni^{2+} specieses via the interfacial Fe^{3+} of iron rusts. In particular, a mass production of 2.968 g iron rusts/$Ni(OH)_2$ catalysts were successfully prepared by using this simple, lowcost yet valid corrosion engineering. This work provides a novel avenue towards large-scale production of efficient OER catalysts by combing with corrosion science, which is beneficial for boosting the progress of water splitting.

Introduction

Hydrogen energy has been regarded as potential substitution of traditional fossil fuels due to the

superiorities of renewability, cleanliness and high energy density.[1-4] Water electrocatalysis is an admirable technique to produce hydrogen by employing the sustainable solar energy and wind energy.[5, 6] As one essential half-reaction of water electrocatalysis, oxygen evolution reaction (OER) has aroused numerous investigations owing to the high reaction barriers. It is notably that OER is a four electron reaction containing the intermediates of OH*, O* and OOH*, which results in the sluggish kinetics.[7-10] To overcome high overpotentials of OER, developing highly active and durable electrocatalysts seems necessary. Compared with precious metal catalysts (such as IrO_2 and RuO_2), transition metal based catalysts have received much wider considerations because of their low cost, structural diversity, good designability and excellent activity.[11]

In general, electrocatalytic reaction occurs on the surface of catalysts and thus the surface sites are more essential in contrast with the bulk sites. Actually, the edges and defects are always considered as the genuine origin of electrocatalysts.[12-15] Thus, there are many works exploiting the construction of high surface area and abundant porous channels to increase the numbers of edges and defects, leading to the promotion of OER activity.[16-19] Different from the traditional approaches, recent advances have revealed that the interfacial interaction between two divergent phases is also conductive to the improvement of OER activity.[20, 21] For example, the OER activity of Ni-Fe layered double hydroxide was availably enhanced through regulating electronic structure via the formed surface FeOOH nanoparticles.[22] Fabricating $FeNi_3$ nanosheet-covered FeOOH arrays is profitable for achieving excellent OER activity by the interfacial interaction of $FeNi_3$-FeOOH Mott–Schottky architecture.[23] Especially, physically mixing Ni and Fe based oxyhydroxides has been also proved to be an effective approach to obtain efficient OER catalysts through forming interfacial Ni-(O)-Fe species in the direct contact areas.[24] Therefore, depending on the interfacial interaction supplies a promising perspective to prepare high-performance OER catalysts. In addition, large-scale preparation is indispensable for the practical application of electrocatalysts, which requires the lowcost raw materials, simple synthesis process and available control to decrease the production cost. However, the usually applied synthesis approaches of top-down (such as exfoliation) and bottom-up (such as hydrothermal preparation) require extra thermal energy input and complex operating steps, which inevitably increase production cost and decrease controllability of catalysts.[25-27] Therefore, exploiting novel facile synthesis strategy is urgent for large-scale preparation of OER electrocatalysts.

Iron corrosion is a common phenomenon that happens on the surface of iron-based devices, which causes their performance degradation and affects normal running. Therefore, iron corrosion undoubtedly results in a huge loss to the economy development.[28] Many reports have confirmed that iron corrosion can be aggravated by the incorporation of chloride ions (Cl^-) owing to the serious breakdown of passive films.[29, 30] Actually, iron corrosion is an electrochemical process with electron gain and loss, while Fe is oxidized to produce the Fe-oxyhydroxide phase (FeOOH), namely iron rusts.[31] As we know Fe-oxyhydroxide is an important component of NiFe-based catalysts, which may be employed in the fabrication of OER catalysts.[32, 33] It will achieve the aim of turning useless iron rusts into useful OER catalysts. However, there is no previous investigation employing iron rusts in the preparation of OER catalysts until now.

Inspired by the purpose of upcycling "waste" (iron rusts) into "wealth" (OER catalysts), we propose a novel corrosion engineering in this work to fabricate hierarchical iron rusts/$Ni(OH)_2$ nanosheet-on-microsphere arrays as OER catalysts. The ultrathin iron rusts were prepared by taking the advantage of accelerated oxygen corrosion by Cl^- species and the contents of iron rusts increased as the enlarged reaction times. Through physically mixing iron rusts with $Ni(OH)_2$ microspheres, the OER activity of $Ni(OH)_2$ has been remarkably improved due to the formed oxygen bridges of Fe^{3+}-O-Ni on the solid-solid contact sites. The optimized iron rusts/$Ni(OH)_2$ catalyst requires a low overpotential of 318 mV to reach the current density of 20 mA cm^{-2} as well as continuously stable operation for 30 h. Specially, a mass production of 2.968 g iron rusts/$Ni(OH)_2$ catalysts was also successfully achieved. This simple and lowcost corrosion-assisted method is beneficial for promoting the development of OER catalysts.

Experimental

Materials

Fe foam was bought from Kunshan Tengerhui electronic technology Co., LTD. $NiSO_4 \cdot 6H_2O$, NaOH, $(NH_4)_2SO_4$, NaCl and KOH was purchased from Sinopharm Chemical Reagent Co., Ltd. Deionized water was applied throughout this work.

Preparation of $Ni(OH)_2$ microspheres

$Ni(OH)_2$ microspheres were prepared by a liquid phase precipitation method. Firstly, 1 M $NiSO_4 \cdot 6H_2O$ solution and 2 M NaOH solution were configured in deionized water. 8 g $(NH_4)_2SO_4$

was dissolved in 80 mL of deionized water to obtain a transparent solution with vigorous stirring at 50 °C. The $NiSO_4 \cdot 6H_2O$ and NaOH solutions were dropwise added into the $(NH_4)_2SO_4$ solution while the pH value was remained as 10. After the reaction was over, the final precipitations were washed with water for several times and dried at 60 °C for 24 h.

Preparation of iron rusts/$Ni(OH)_2$ catalysts

The iron rusts/$Ni(OH)_2$ catalysts were synthesized via a facile corrosion engineering. Firstly, Fe foam with the size of 2×2 cm^2 was placed in 30 mL of 5 mM NaCl solution with continuous stirring for 60 min to obtain the solution A with iron rusts. After the corrosion reaction, Fe foam was taken out from the solution A. 300 mg of $Ni(OH)_2$ microspheres were dispersed uniformly in 10 mL water by ultrasonic treatment to gain the solution B. Then, the solution B was added into the solution A drop by drop and the mixtures were stirred for another 30 min after ultrasonic treatment for 20 min. The mixed solution was kept in quiescence and the supernatant liquor was removed. 30 mL water was again added in the products and kept in quiescence. This process was repeated for 3 times and the precipitates were dried under vacuum at 60 °C for 12 h to achieve the final product of iron rusts/$Ni(OH)_2$. To optimize OER performances, the catalysts with different corrosion time of Fe foams in NaCl solution were prepared for 30, 90 and 120 min. The samples treated in 5 mM NaCl solution without FF ($Ni(OH)_2$-NaCl) and in deionized water with Fe foam ($Ni(OH)_2$-FF) were synthesized for contrast.

For the large-scale preparation of iron rusts/$Ni(OH)_2$ catalysts, the corrosion reaction was performed in 300 mL of 5 mM NaCl solution with 10 pieces of Fe foam (2×2 cm^2) for 60 min. 3 g $Ni(OH)_2$ microspheres were employed by dispersing in 100 mL water. The mass of the finally gained product was determined to be 2.968 g.

Preparation of Ni/MoO_2 as cathodic HER catalyst

The Ni/MoO_2 catalyst was prepared as the cathodic HER catalyst according to our previous work.[34] Concretely, 457.6 mg (2 mmol) $Ni(NO_3)_2 \cdot 6H_2O$ was firstly added into 30 mL deionized water as well as 600 mg (10 mmol) urea and 483.8 mg (2 mmol) $NaMoO_4 \cdot 2H_2O$. Then, the transparent solution was poured in a 50 mL Teflon-lined stainless steel autoclave and kept at 150 °C for 12 h. After being washed with water and alcohol, the obtained precipitates were dried at 60 °C and calcined at 400 °C for 2 h in the Ar/H_2 atmosphere. The final product is the Ni/MoO_2 catalyst.

Characterization of iron rusts/$Ni(OH)_2$ catalysts

Physical characterization. The phases of catalysts were tested via an X' Pert PRO X-ray diffraction (XRD) device. Morphologies were determined through a Sirion200 Field Emission Scanning Electron Microscope (SEM) as well as a Tecnai G2 F20 Transmission Electron Microscope (TEM). In addition, an AXIS-Ultra DLD-600W device was employed to gain the X-ray photoelectron spectroscopy (XPS) spectra.

Electrochemical characterization. The electrocatalytic performances were determined via an Autolab PG302N electrochemical workstation by employing a three-electrode system. The glassy carbon electrode with diameter of 5 mm, self-made reversible hydrogen electrode (RHE) and graphite rod were utilized as the working, reference and counter electrode, respectively. The ink was prepared by dispersing 5 mg catalyst in 1 mL 0.1% Nafion/isopropanol solution, and then 16.5 μL ink was dropped on the glassy carbon electrode to prepare the working electrode with the loading amount of 0.42 mg cm^{-2}. Linear sweep voltammetry (LSV) curves were detected in O_2-saturated 1.0 M KOH solution from 1.0 V to 1.8 V. The electrochemical impedance spectroscopy (EIS) of catalysts was tested with the frequency range of 0.01 Hz-0.1 M Hz. Cyclic voltammetry (CV) curves were determined in the potential range of 0.75-0.85 V at a series scanning rates of 20, 40, 60, 80, 100 and 120 mV s^{-1}. Besides, the OER operation stability was performed by the chronopotentiometric at the current density of 10 mA cm^{-2}. The overall water splitting device was assembled by the as-prepared iron rusts/$Ni(OH)_2$ and Ni/MoO_2 as anodic and cathodic catalysts, respectively. 100 μL inks were painted on 0.5×0.5 cm^2 Ni foam to achieve the loading amount of 2 mg cm^{-2}. LSV curve was determined in the potential range of 1.0-1.8 V. The operate durability was performed by the chronopotentiometry measurement at 20 mA cm^{-2}.

Results and discussion

The iron rusts/$Ni(OH)_2$ catalysts with hierarchical nanosheet-on-microsphere arrays were synthesized through a facile corrosion engineering, as shown in **Scheme 1**. Firstly, the ultrathin iron rust nanosheets were prepared by immersing Fe foam in 5 mM NaCl solution with vigorous stirring, showing an oxygen corrosion process. The generated iron rusts naturally fall off from the surface of Fe foam in the stirring process. Next, iron rusts were physically mixed with hierarchical $Ni(OH)_2$ microspheres to obtain the iron rusts/$Ni(OH)_2$ catalysts. The solid-solid interface

interaction with oxygen bridges of Fe-O-Ni is expected to improve the OER activity of catalysts.

Scheme 1. Schematic illustration of preparing the iron rusts/$Ni(OH)_2$ catalysts.

The fabrication and characterization of iron rusts are investigated as shown in **Fig. 1**. For better understanding the generating mechanism of iron rusts, Fe foams in deionized water and 5 mM NaCl solution are compared as depicted in **Fig. 1a-b**. It is clear that there has almost no change for Fe foam treated in water, while the color becomes yellow for NaCl solution because of the generated iron rusts. Besides, it is observed from the photos of Fe foam after reaction (**Fig. S1**) that there is a spot of rusts on the surface of Fe foam in water, but the surface of Fe foam in 5 mM NaCl is thoroughly corroded, further revealing the successful corrosion in NaCl solution. The result proves that the corrosion process has been significantly enhanced by the NaCl solution, which is mainly due to the high depassivation of Cl^- ions.[35] The XRD pattern in **Fig. 1c** shows that iron rusts exhibit the single phase of γ-FeOOH (PDF-73-2326). The morphologies were determined by SEM and TEM techniques in **Fig.1d-e** and it is found that iron rusts display appealing three-dimension nanosheet arrays. The selective area electron diffraction in **Fig. 1f** exhibits the bright rings are attributed to the (021), (130), (150), (170) and (260) crystal planes of FeOOH. The average thickness of the FeOOH nanosheets was detected to be 4.02 nm by AFM technique in **Fig. 1g**, revealing ultrathin structures to expose sufficient interaction sites. The EDX elemental mapping images show the uniform dispersion of Fe and O atoms (**Fig. 1h-j**). In addition, according to the neutral pH value of NaCl solution, the occurred corrosion here is belonging to oxygen corrosion. Actually, Fe atoms loss electrons to generate Fe^{2+} in the nanoscale cathodic regions, while oxygen gas dissolved in the solution can receive the electrons to produce hydroxyl groups (OH^-) in the anodic regions.[36] As a result, the formed Fe^{2+} ions react with OH^- to generate the $Fe(OH)_2$ nanosheets, which is further oxidized to γ-FeOOH (**Fig. 1k**) as the following

equations:

$$Fe \leftrightarrow Fe^{2+} + 2e^- \quad (1)$$

$$O_2 + 2H_2O + 4e^- \leftrightarrow 4OH^- \quad (2)$$

$$Fe^{2+} + 2OH^- \leftrightarrow Fe(OH)_2 \downarrow \quad (3)$$

$$Fe(OH)_2 + OH^- \leftrightarrow \gamma\text{-}FeOOH + H_2O + e^- \quad (4)$$

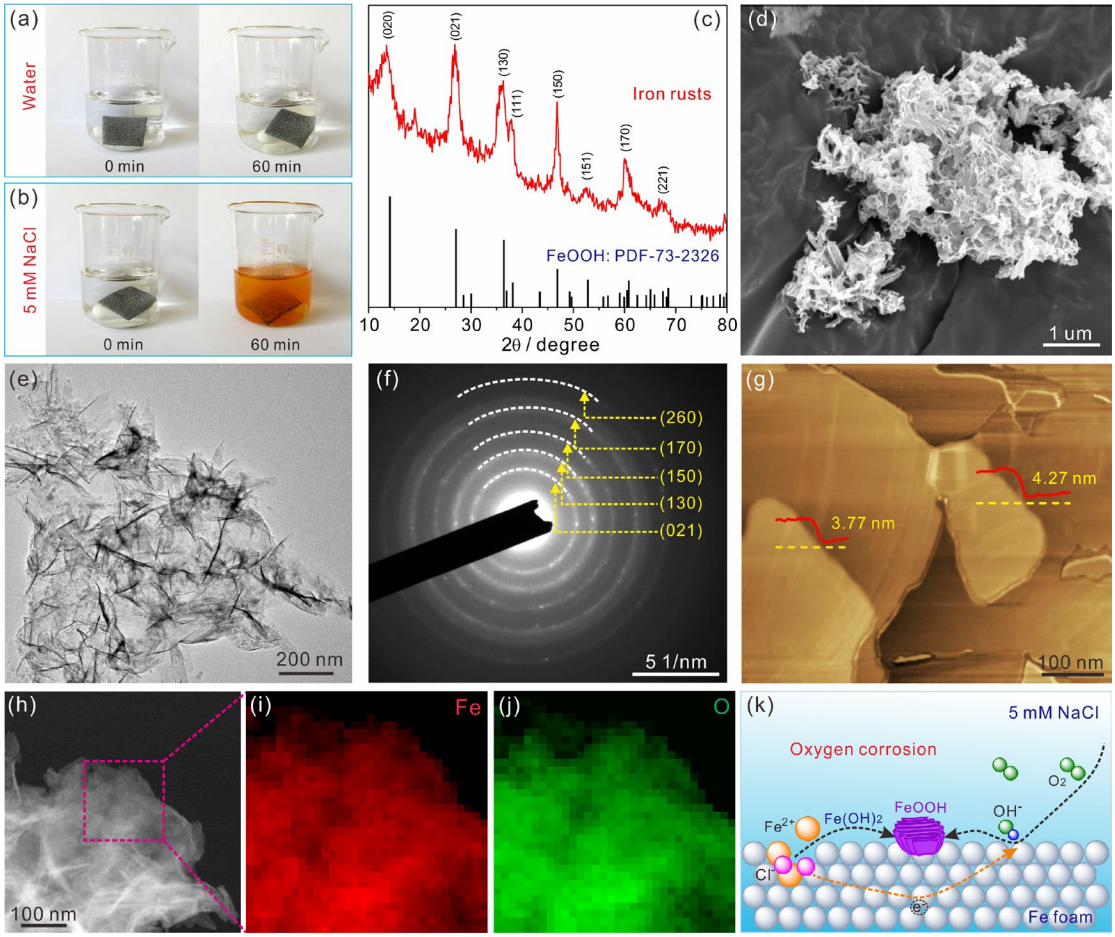

Fig. 1. Photos of Fe foam treated in (a) deionized water and (b) 5 mM NaCl solution; compositions and morphologies of iron rusts: (c) XRD pattern, (d) SEM image, (e) TEM image, (f) selective area electron diffraction pattern, (g) AFM image and (h-j) EDX elemental mapping images; (k) corrosion mechanism of Fe foam to produce iron rusts.

Hierarchical $Ni(OH)_2$ microspheres were then utilized to achieve the iron rusts/$Ni(OH)_2$ catalysts. XRD pattern in **Fig. 2a** exhibits that these microspheres contain a pure $Ni(OH)_2$ phase (PDF-73-1520). The morphologies in **Fig. 2b** and **Fig. S2** reveal that uniform microspheres with numerous nanosheets are fabricated, which are beneficial for providing abundant contacted sites. After physically mixing iron rusts with $Ni(OH)_2$ microspheres, the iron rusts/$Ni(OH)_2$ catalyst was

fabricated accordingly. Iron rusts with different corrosion time were employed to optimize OER performances and the phase compositions of these catalysts are evaluated by the XRD patterns in **Fig. 2c**. It is observed that the strong peaks are corresponding to the $Ni(OH)_2$ phase, while there is a weak peak sign at 27.1° for the catalyst with 120 min corrosion belonging to the FeOOH phase. The weak XRD peaks are attributed to the small amount of imported iron rusts. The chemical compositions were further revealed by XPS analysis and the survey spectrum in **Fig. S3** shows the presence of Fe, Ni and O elements. The Ni spectrum in **Fig. 2d** can be resolved into five peaks. The main peak at 855.32 eV belongs to Ni 2p3/2 as well as two satellite peaks at 860.69 eV and 863.84 eV. The other peak at 872.88 eV with one satellite peak of 879.24 eV is indexed to Ni 2p1/2. The Fe spectrum in **Fig. 2e** displays that the peak located at 711.72 eV with two satellite peaks of 706.7 eV and 715.98 eV is ascribed to Fe 2p3/2, while the peak located at 723.26 eV is corresponding to Fe 2p1/2, which coincides with the feature of Fe^{3+} from iron rusts.[37] The O spectrum in **Fig. 2f** has a strong peak at 530.41 eV belonging to O 1s with a weak peak at 531.36 eV ascribed to M-O species (M = Fe, Ni). The above results confirm that the iron rusts/$Ni(OH)_2$ catalysts were successfully fabricated.

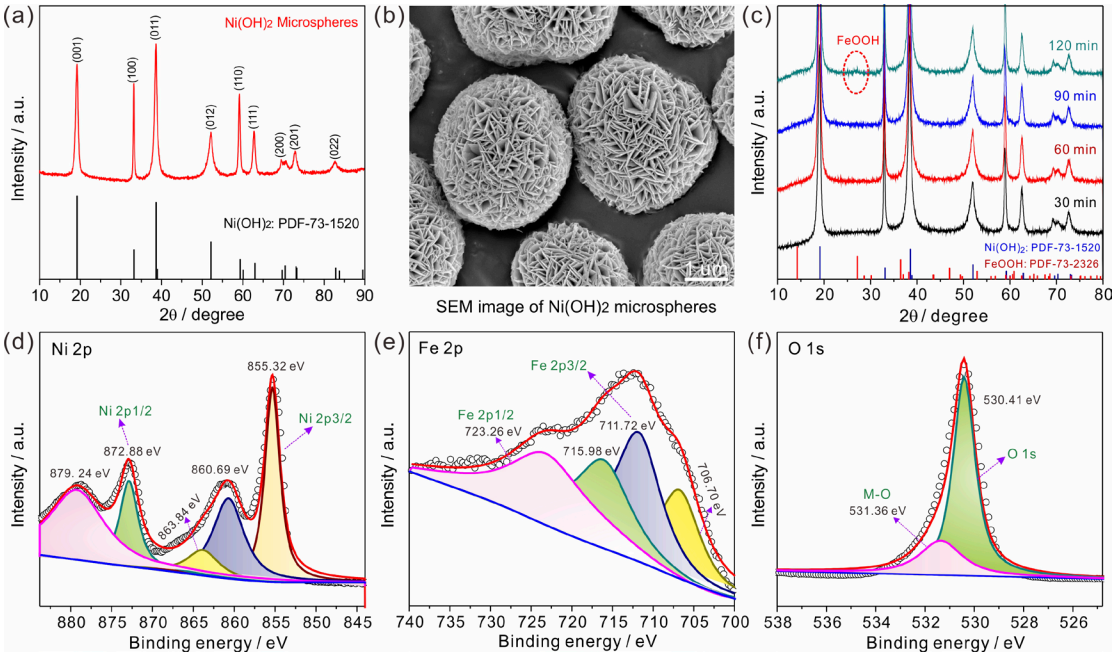

Fig. 2. (a) XRD pattern and (b) SEM image of the $Ni(OH)_2$ microspheres, (c) XRD patterns of iron rusts/$Ni(OH)_2$ catalysts obtained with different corrosion time; XPS spectra of iron rusts/$Ni(OH)_2$: (d) Ni 2p spectrum, (e) Fe 2p spectrum and (f) O 1s spectrum.

All the electrocatalytic performances were determined via a three-electrode system in 1.0 M

KOH electrolyte. Firstly, the influence of corrosion time has been exploited to optimize the electrochemical activity. **Fig. 3a** shows the photographs of Fe foam in 5 mM NaCl solution with different corrosion time. As the reaction time increases from 30 min to 120 min, the color of NaCl solutions gradually becomes dark owing to the augmented amounts of iron rusts. The weights of iron rusts after being dried are determined as shown in **Fig. 3b** and it is clearly found that a stepwise increasement is achieved with increasing corrosion time. Such small amount is correlated to the ultrathin nanosheet arrays of iron rusts. Electrochemical measurements in **Fig. 3c** show that the catalyst with corrosion time of 60 min has the best OER performance, which requires a low overpotential of 318 mV to receive the current density of 20 mA cm^{-2}. The overpotentials at 20 and 50 mA cm^{-2} are also compared in **Fig. 3d.** A trend of down first and then up is observed for these iron rusts/$Ni(OH)_2$ catalysts, which is correlated to the increased weights of iron rusts. The higher amount of iron rusts can impede the uniform blending of the iron rusts/$Ni(OH)_2$ catalysts, hindering the exposure of accessible active sites.

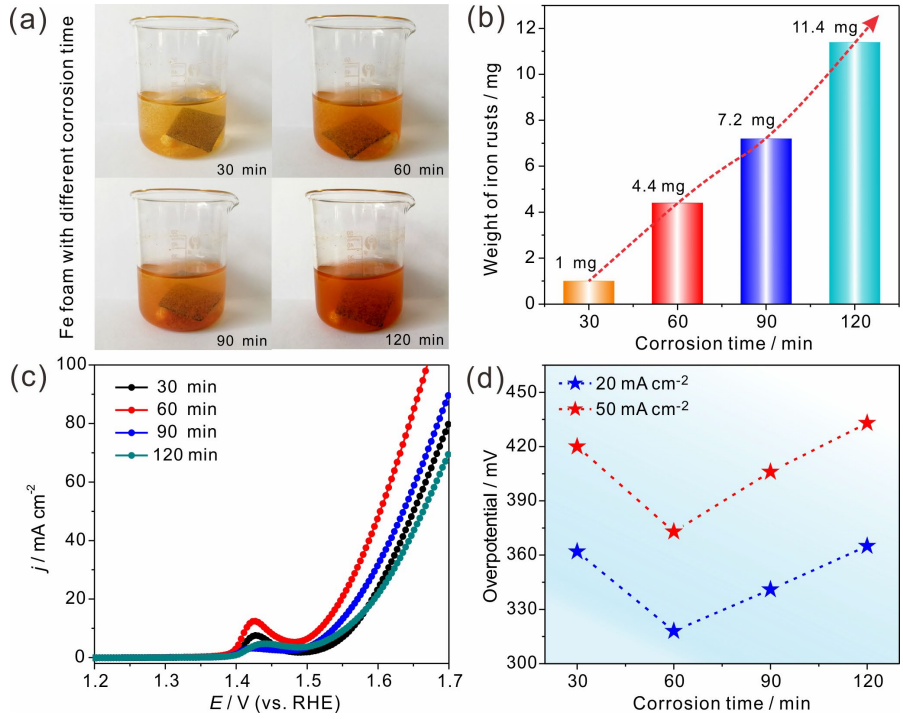

Fig. 3. (a) Photographs of Fe foam in NaCl solution with different reaction times, (b) the corresponding weight of iron rusts, electrocatalytic performances of catalysts obtained with different corrosion time: (c) polarization curves and (d) comparison of overpotentials at the current density of 20 mA cm^{-2} and 50 mA cm^{-2}.

As discussed above, the iron rusts/$Ni(OH)_2$ catalyst synthesized with corrosion time of 60

min exhibits the optimized OER activity, which is further compared with $Ni(OH)_2$, iron rusts and Ir/C in **Fig. 4**. The polarization curves in **Fig. 4a** display that iron rusts/$Ni(OH)_2$ possesses the highest OER activity among these catalysts. By comparing the overpotentials at the current density of 20 mA cm^{-2} and 50 mA cm^{-2} in **Fig. 4b**, it is notably that obviously lower overpotentials are achieved for iron rusts/$Ni(OH)_2$, which only needs the overpotentials of 318 and 373 mV, respectively. The result confirms that the OER activity of $Ni(OH)_2$ microspheres has been remarkably promoted by the simply physical mixing with iron rusts. To further confirm the OER activity, polarization curves of $Ni(OH)_2$-NaCl and $Ni(OH)_2$-FF were also detected in **Fig. S4**. It indicates that there is no difference of OER activity between pristine $Ni(OH)_2$ and $Ni(OH)_2$-NaCl, proving that NaCl solution has no effect on OER activity. The OER activity of $Ni(OH)_2$-FF has been slightly improved, which is attributed to the mild corrosion of Fe foam in water. However, the activity enhancement for $Ni(OH)_2$-FF is very little, further confirming the validity of activity reinforce for iron rusts/$Ni(OH)_2$. Tafel slope is an essential parameter of describing the reaction mechanism of catalysts, which is calculated according to the Tafel equation: $\eta = b\log j + a$ (η is the overpotential, j represents the current density and b belongs to the Tafel slope). **Fig. 4c** exhibits that the lowest Tafel slope of 92.7 mV dec^{-1} is achieved for iron rusts/$Ni(OH)_2$, which is much lower than those of Ir/C (99.9 mV dec^{-1}), FeOOH (103.8 mV dec^{-1}) and $Ni(OH)_2$ (128.3 mV dec^{-1}), revealing a quick oxygen evolution mechanism. The impedance values achieved from the Nyquist plots in **Fig. 4d** depict that iron rusts/$Ni(OH)_2$ has a lower R_{ct} value of 24 Ω than those of $Ni(OH)_2$ and FeOOH, indicating the fastest electron transfer mechanism of OER on iron rusts/$Ni(OH)_2$. To get insight into the OER activity, the electrochemical double-layer capacitance (Cdl) which is in direct proportion to the electrochemical active surface area (ECSA)[38] is calculated from the CV curves in **Fig. S5**. It is worth noting that a Cdl value of 0.39 mF cm^{-2} is received for iron rusts/$Ni(OH)_2$, which is superior to those of $Ni(OH)_2$ (0.25 mF cm^{-2}) and FeOOH (0.33 mF cm^{-2}) (**Fig 4e**). The accordingly higher ECSA of iron rusts/$Ni(OH)_2$ is mainly ascribed to the special nanosheet-on-microsphere arrays. Moreover, excellent stability is necessary for the practical application of OER catalysts. **Fig 4f** exhibits that the iron rusts/$Ni(OH)_2$ catalyst continuously operates for 30 h without obvious attenuation at the current density of 10 mA cm^{-2}, confirming the promising stability. These results indicate that the as-prepared iron rusts/$Ni(OH)_2$ catalyst is profitable for employment in water electrocatalysis.

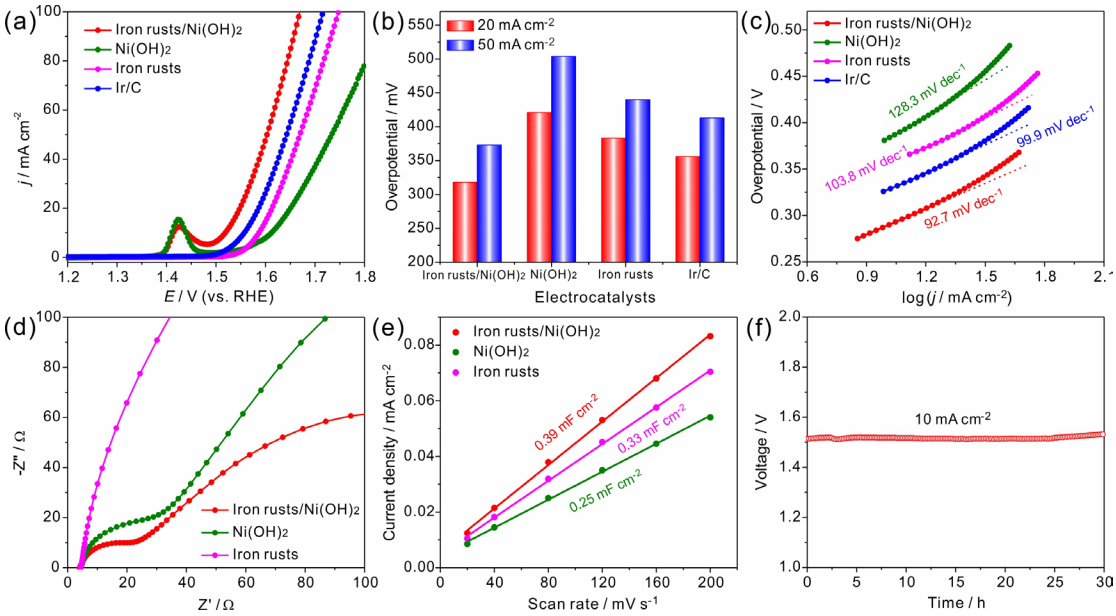

Fig. 4. Electrocatalytic performances of iron rusts/$Ni(OH)_2$, $Ni(OH)_2$, iron rusts and Ir/C: (a) polarization curves, (b) comparison of overpotentials at the current density of 20 mA cm^{-2} and 50 mA cm^{-2}, (c) corresponding Tafel slopes, (d) Nyquist plots, (e) Cdl values at various scanning rates, (f) chronopotentiometric curve at the current density of 10 mA cm^{-2}.

To elucidate the electrocatalytic mechanism, SEM images of iron rusts/$Ni(OH)_2$ catalyst were determined in **Fig. 5a-c**. Compared with $Ni(OH)_2$ microspheres (**Fig. S2b-c**), there are some iron rust nanosheets dispersed on the $Ni(OH)_2$ spheres for iron rusts/$Ni(OH)_2$ catalyst, exhibiting special nanosheet-on-microsphere arrays. In consideration of the facile physical mixing, the compositions and morphologies of iron rusts and $Ni(OH)_2$ have not been changed in the synthesis process, while there are new solid-solid interfaces formed between iron rusts and $Ni(OH)_2$. It is noted that the interfacial oxygen bridges of Fe-O-Ni can be accordingly generated on the solid-solid contact sites. Such Fe-O-Ni species are profitable for regulating the interfacial electronic structures of iron rusts/$Ni(OH)_2$ catalysts and thus improving the OER activity.[24] Besides, recent reports[23] have demonstrated that the surface Fe^{3+} ions are beneficial for enhancing the OER activity of Ni^{2+} through promoting the oxidation of Ni^{2+} ($Ni^{2+}\rightarrow Ni^{3+}/Ni^{4+}+e^-$). Therefore, the Fe-O-Ni species with Fe^{3+} from ultrathin iron rusts can favorably accelerate the production of high valent state Ni ions, leading to a fast oxygen evolution process (**Fig. 5d**). To further confirm the regulated electronic structure of Ni^{2+} ions, the first CV curves of iron rusts/$Ni(OH)_2$, $Ni(OH)_2$ and iron rusts were detected in **Fig. 5e**. It is clearly observed that the backward scans all possess higher current density than those of the forward scans, which are caused by the activation effect in

the forward oxidation process.[22] The potential differences (Δη) at the same current density of 10 mA cm^{-2} and 20 mA cm^{-2} are calculated and compared in **Fig. 5f**. It can be found that the largest values of 30 and 23 mV are achieved for iron rusts/$Ni(OH)_2$ among the three catalysts, which are mainly attributed to the activation effect of the Fe-O-Ni species on the solid-solid interface sites. Different from the traditional catalysts with edges and defects as active sits, the formed oxygen bridges of Fe-O-Ni provides a diverse perspective for preparing efficient OER catalysts.

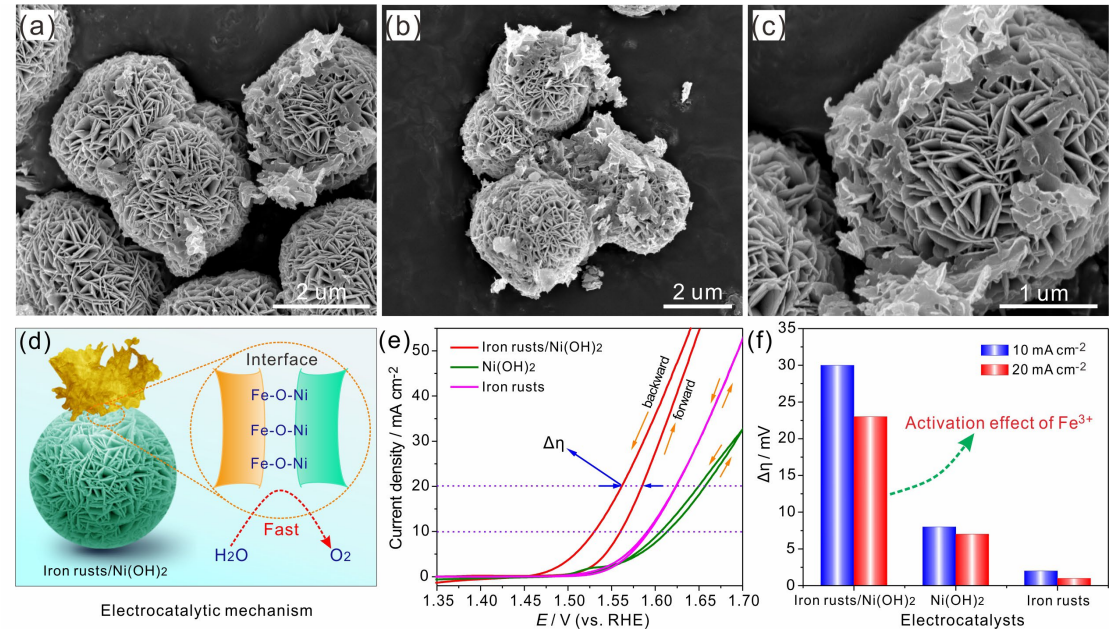

Fig. 5. (a-c) SEM images of iron rusts/$Ni(OH)_2$ catalyst, (d) electrocatalytic mechanism of iron rusts/$Ni(OH)_2$ catalyst for enhanced OER activity, (e) the first CV curves of iron rusts/$Ni(OH)_2$, $Ni(OH)_2$ and iron rusts catalysts, (f) comparison of potential differences at the current density of 10 mA cm^{-2} and 20 mA cm^{-2}.

The water splitting application of iron rusts/$Ni(OH)_2$ catalyst was employed in 1.0 M KOH electrolyte. Another non-precious metal Ni/MoO_2 catalyst was synthesized as the cathodic HER catalyst and the polarization curve depicted in **Fig. 6a** shows that Ni/MoO_2 contains excellent activity of requiring a low overpotential of 35 mV to reach the 10 mA cm^{-2} current density. The water splitting cell assembled by iron rusts/$Ni(OH)_2$ and Ni/MoO_2 catalysts can derive the current density of 10, 20 and 50 mA cm^{-2} at the voltage of 1.55, 1.62 and 1.71 V (**Fig. 6b-c**), respectively, which is superior to many reported values in **Table S1**.[39-43] Long-term stable operation is essential for water electrocatalysis. The stability of overall water splitting device was also performed in **Fig. 6d** and it can continuously work at the current density of 20 mA cm^{-2} for 24 h with no performance

degradation. It confirms that the synthesized iron rusts/$Ni(OH)_2$ catalyst is a potential candidate for water splitting.

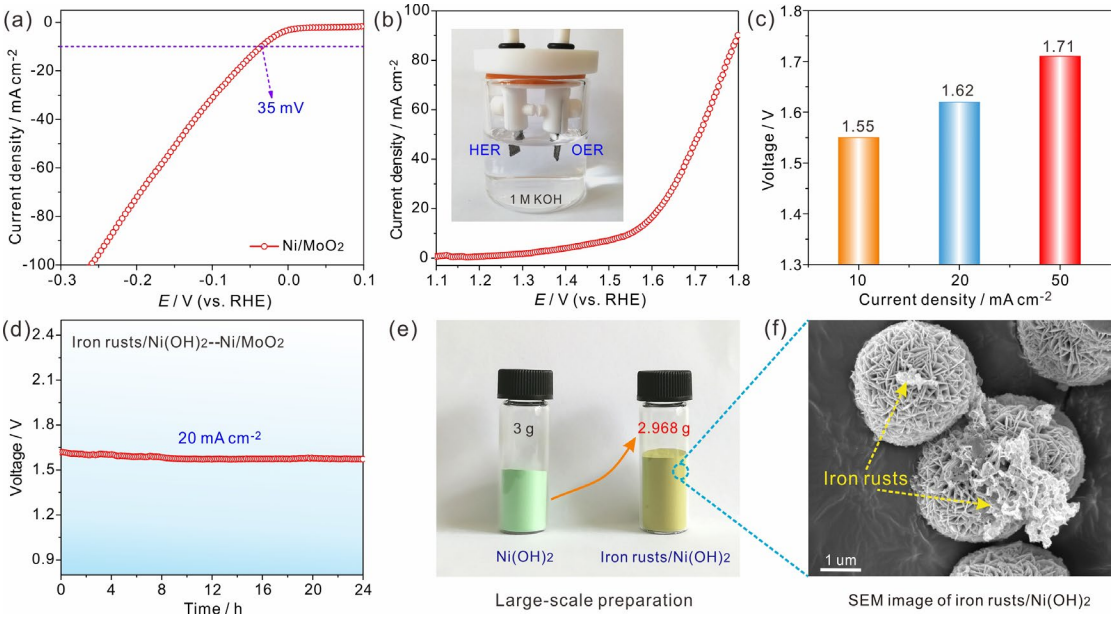

Fig. 6. (a) Polarization curves of Ni/MoO_2 catalyst in 1.0 M KOH electrolyte, (b) polarization curve of the assembled water splitting cell by iron rusts/$Ni(OH)_2$ and Ni/MoO_2 catalysts (inset: the water splitting device), (c) voltages of water splitting cell at different current densities, (d) the stability determination at the constant current density of 20 mA cm^{-2}, (e) the large-scale preparation of iron rusts/$Ni(OH)_2$ and (f) the corresponding SEM image.

Owing to the simple and facile procedure of corrosion engineering, the hierarchical iron rusts/$Ni(OH)_2$ catalyst is easy to scale up on the gram level. Actually, 10 pieces of Fe foam in 300 mL NaCl solution were vigorously stirred with adding 3 g $Ni(OH)_2$ microspheres and the weight of final product was detected to be 2.968 g. A small amount of weight loss occurs inevitably in the preparation process. **Fig. 6e** shows the photographs of initial $Ni(OH)_2$ and prepared iron rusts/$Ni(OH)_2$ catalysts. It is notably that much larger volume is obtained for iron rusts/$Ni(OH)_2$ than $Ni(OH)_2$ because of the introduced loose and ultrathin iron rusts. The SEM image in **Fig. 6f** displays the hierarchical iron rusts/$Ni(OH)_2$ nanosheet-on-microsphere arrays of the synthesized catalyst. The above result reveals that the large-scale preparation of iron rusts/$Ni(OH)_2$ catalyst is successfully achieved, further confirming the appealing application in water electrocatalysis.

Conclusions

In conclusion, a novel corrosion engineering has been demonstrated to prepare hierarchical iron

rusts/$Ni(OH)_2$ nanosheet-on-microsphere arrays as excellent OER catalyst. The ultrathin iron rusts were obtained by employing the accelerated oxygen corrosion of Fe foam in 5 mM NaCl solution. By physically mixing iron rusts with $Ni(OH)_2$ microspheres, the achieved catalyst exhibits remarkable OER activity of requiring a low overpotential of 318 mV to derive the current density of 20 mA cm^{-2} as well as continuously stable operation for 30 h. The enhanced electrocatalytic activity of iron rusts/$Ni(OH)_2$ is mainly attributed to the formed oxygen bridges of Fe-O-Ni on the solid-solid interfaces. The water splitting cell assembled by the iron rusts/$Ni(OH)_2$ and Ni/MoO_2 catalysts can derive 20 mA cm^{-2} at the low voltage of 1.62 V and stably work for 24 h. Moreover, a large-scale preparation of 2.968 g iron rusts/$Ni(OH)_2$ catalyst was successfully achieved by utilizing the simple and lowcost corrosion engineering. By combining with corrosion science, this work puts forward an effective strategy to synthesize promising OER catalysts, which is believed to expedite the development of water electrocatalysis.

Conflicts of interest

There are no conflicts to declare.

Acknowledgements

This work was supported by the National Natural Science Foundation (91963109) and the China Postdoctoral Science Foundation (2019M662583). The authors thank the Analytical and Testing Center of HUST for allowing use of its facilities.

Notes and references

1 K. Wang, X. She, S. Chen, H. Liu, D. Li, Y. Wang, H. Zhang, D. Yang and X. Yao, *J. Mater. Chem. A*, 2018, **6**, 5560-5565.
2 D. Dong, Z. Wu, J. Wang, G. Fu and Y. Tang, *J. Mater. Chem. A*, 2019, **7**, 16068-16088.
3 G. Huang, Z. Xiao, R. Chen and S. Wang, *ACS Sustain. Chem. Eng.*, 2018, **6**, 15954-15969.
4 P. Wang, Z. Pu, W. Li, J. Zhu, C. Zhang, Y. Zhao and S. Mu, *J. Catal.*, 2019, **377**, 600-608.
5 X. Liu, S. Deng, D. Xiao, M. Gong, J. Liang, T. Zhao, T. Shen and D. Wang, *ACS Appl. Mater. Interfaces*, 2019, **11**, 42233-42242.
6 I. S. Amiinu, Z. Pu, D. He, H. G. R. Monestel and S. Mu, *Carbon*, 2018, **137**, 274-281.
7 Y. Wang, M. Qiao, Y. Li and S. Wang, *Small*, 2018, **14**, e1800136.
8 H. Wang, E. Feng, Y. Liu and C. Zhang, *J. Mater. Chem. A*, 2019, **7**, 7777-7783.
9 Y. Zou, Z. Liu, R. Liu, D. Liu, C. Dong, Y. Wang and S. Wang, *J. Power Sources*, 2019, **427**, 215-222.
10 D. Wang, Z. Liu, S. Du, Y. Zhang, H. Li, Z. Xiao, W. Chen, R. Chen, Y. Wang, Y. Zou and S. Wang, *J. Mater. Chem. A*, 2019, **7**, 24211-24216.

11 Y. Yang, L. Dang, M. J. Shearer, H. Sheng, W. Li, J. Chen, P. Xiao, Y. Zhang, R. J. Hamers and S. Jin, *Adv. Energy Mater.*, 2018, **8**, 1703189.

12 P. Zhou, J. He, Y. Zou, Y. Wang, C. Xie, R. Chen, S. Zang and S. Wang, *Sci. China Chem.*, 2019, **62**, 1365-1370.

13 Y. Wang, L. Tao, Z. Xiao, R. Chen, Z. Jiang and S. Wang, *Adv. Funct. Mater.*, 2018, **28**, 1705356.

14 Z. Xiao, Y. Wang, Y. Huang, Z. Wei, C. Dong, J. Ma, S. Shen, Y. Li and S. Wang, *Energ. Environ. Sci.*, 2017, **10**, 2563-2569.

15 J. Zhang, Y. Sun, J. Zhu, Z. Gao, S. Li, S. Mu and Y. Huang, *Adv. Sci.*, 2018, **5**, 1801375.

16 W. Wang, Y. Liu, J. Li, J. Luo, L. Fu and S. Chen, *J. Mater. Chem. A*, 2018, **6**, 14299-14306.

17 H.-F. Wang, R. Chen, J. Feng, M. Qiao, S. Doszczeczko, Q. Zhang, A. B. Jorge and M.-M. Titirici, *ChemElectroChem*, 2018, **5**, 1786-1804.

18 Y. Li, F. Li, X. Meng, S. Li, J. Zeng and Y. Chen, *ACS Catal.*, 2018, **8**, 1913-1920.

19 X. Liu, S. Deng, P. Liu, J. Liang, M. Gong, C. Lai, Y. Lu, T. Zhao and D. Wang, *Sci. Bull.*, 2019, **64**, 1675-1684.

20 J. Wu, Z. Ren, S. Du, L. Kong, B. Liu, W. Xi, J. Zhu and H. Fu, *Nano Res.*, 2016, **9**, 713-725.

21 H. Zhang, X. Li, A. Hähnel, V. Naumann, C. Lin, S. Azimi, S. L. Schweizer, A. W. Maijenburg and R. B. Wehrspohn, *Adv. Funct. Mater.*, 2018, **28**, 1706847.

22 J. Chen, F. Zheng, S. Zhang, A. Fisher, Y. Zhou, Z. Wang, Y. Li, B. Xu, J. Li and S. Sun, *ACS Catal.*, 2018, **8**, 11342-11351.

23 H. Meng, Z. Ren, S. Du, J. Wu, X. Yang, Y. Xue and H. Fu, *Nanoscale*, 2018, **10**, 10971-10978.

24 M. Gorlin, P. Chernev, P. Paciok, C. W. Tai, J. Ferreira de Araujo, T. Reier, M. Heggen, R. Dunin-Borkowski, P. Strasser and H. Dau, *Chem. Commun.*, 2019, **55**, 818-821.

25 Y. Kang, H. Xie, D. Liu, M. Gao, P. K. Chu, S. Ramakrishna and X. F. Yu, *Chem. Commun.*, 2019, **55**, 11406-11409.

26 Z. Kou, T. Wang, Z. Pu, L. Wu, K. Xi and S. Mu, *Nanoscale Horiz.*, 2019, **4**, 196-201.

27 L. Wang, Q. Zhou, Z. Pu, Q. Zhang, X. Mu, H. Jing, S. Liu, C. Chen and S. Mu, *Nano Energy*, 2018, **53**, 270-276.

28 B. Zhang, J. Wang, B. Wu, X. W. Guo, Y. J. Wang, D. Chen, Y. C. Zhang, K. Du, E. E. Oguzie and X. L. Ma, *Nat. Commun.*, 2018, **9**, 2559.

29 B. Zhang, X. X. Wei, B. Wu, J. Wang, X. H. Shao, L. X. Yang, S. J. Zheng, Y. T. Zhou, Q. Q. Jin, E. E. Oguzie and X. L. Ma, *Corros. Sci.*, 2019, **154**, 123-128.

30 B. Zhang and X. L. Ma, *J. Mater. Sci. Technol.*, 2019, **35**, 1455-1465.

31 A. J. Davenport, L. J. Oblonsky, M. P. Ryan and M. F. Toney, *J. Electrochem. Soc.*, 2000, **147**, 2162.

32 H. Bandal, K. K. Reddy, A. Chaugule and H. Kim, *J. Power Sources*, 2018, **395**, 106-127.

33 J. Hu, S. Li, J. Chu, S. Niu, J. Wang, Y. Du, Z. Li, X. Han and P. Xu, *ACS Catal.*, 2019, **9**, 10705-10711.

34 S. Deng, X. Liu, T. Huang, T. Zhao, Y. Lu, J. Cheng, T. Shen, J. Liang and D. Wang, *Electrochim. Acta*, 2019, **324**, 134892.

35 S. Hao, L. Chen, C. Yu, B. Yang, Z. Li, Y. Hou, L. Lei and X. Zhang, *ACS Energy Lett.*, 2019, **4**, 952-959.

36 S. Niu, W. J. Jiang, T. Tang, L. P. Yuan, H. Luo and J. S. Hu, *Adv. Funct. Mater.*, 2019, **29**, 1902180.

37 J. Chi, H. Yu, G. Jiang, J. Jia, B. Qin, B. Yi and Z. Shao, *J. Mater. Chem. A*, 2018, **6**, 3397-3401.

38 S. Liu, H. Wen, G. Ying, Y. Zhu, X. Fu, R. Sun and C. Wong, *Nano Energy*, 2018, **44**, 7-14.

39 Y. Li, H. Li, K. Cao, T. Jin, X. Wang, H. Sun, J. Ning, Y. Wang and L. Jiao, *Energy Storage Mater.*, 2018, **12**, 44-53.

40 C. Xuan, J. Wang, W. Xia, Z. Peng, Z. Wu, W. Lei, K. Xia, H. L. Xin and D. Wang, *ACS Appl. Mater. Interfaces*, 2017, **9**, 26134-26142.

41 L. Zhou, M. Shao, J. Li, S. Jiang, M. Wei and X. Duan, *Nano Energy*, 2017, **41**, 583-590.

42 J. Yu, Q. Li, Y. Li, C. Xu, L. Zhen, V. P. Dravid and J. Wu, *Adv. Funct. Mater.*, 2016, **26**, 7644-7651.

43 H. Wang, T. Zhou, P. Li, Z. Cao, W. Xi, Y. Zhao and Y. Ding, *ACS Sustain. Chem. Eng.*, 2017, **6**, 380-388.